INTERNATIONAL JOURNAL FOR NUMERICAL METHODS IN FLUIDS, VOL. 26, 443–457 (1998)

# DIRECT NUMERICAL SIMULATION OF THE AMPLIFICATION OF A 2D TEMPORAL DISTURBANCE IN PLANE POISEUILLE FLOW

G. J. HWANG* AND S. J. WU

*Department of Power Mechanical Engineering, National Tsing Hua University, Hsinchu, 30043, Taiwan*

## SUMMARY

A direct numerical scheme is developed to study the temporal amplification of a 2D disturbance in plane Poiseuille flow. The transient non-linear Navier–Stokes equations are applied in a region of wavelength moving with the wave propagation speed. The complex amplitude involved in the perturbation functions is considered as the initial input of the non-linear stability equations. In this study a fully implicit finite difference scheme with five points in the flow direction and three points in the normal direction is developed so that numerical simulation of the amplification of a two-dimensional temporal disturbance in plane Poiseuille flow can be investigated. The growth and decay of the disturbance with time are presented and neutral stability curves which are in good agreement with existing solutions can be determined. The critical conditions as a function of the amplitude $A_0$ of the disturbance are presented. Fixing the wavelength, the Navier–Stokes equations are solved up to $Re = 10{,}000$ a friction factor increasing with Reynolds number is observed. The 2D non-linear behaviour of the streamfunction, vorticity and velocity components at $Re = 10{,}000$ are also exhibited. © 1998 John Wiley & Sons, Ltd.

*Int. J. Numer. Meth. Fluids*, **26**: 443–457 (1998).

KEY WORDS: direct numerical simulation; 2D temporal disturbance; plane Poiseuille flow; finite difference method; transient non-linear equation; stream-function–vorticity equation

## 1. INTRODUCTION

Although the mathematical theory of the problem of the stability of plane Poiseuille flow to small disturbances for the Orr–Sommerfeld equation has been well developed for many years, the physical mechanism behind the process of instability has received relatively little attention and still remains unclear. In fact, there are a considerable number of phenomena concerning the stability of plane Poiseuille flow which cannot be completely explained by means of the equation of linear hydrodynamic stability. Thus it is interesting and necessary to treat the discrepancy between the results of linear hydrodynamic stability theory and the experimental results, which are non-linear by nature, with regard to the breakdown of laminar flow. Therefore the present study intends to develop a direct numerical scheme to solve the complete time-dependent non-linear Navier–Stokes equations for the stability of plane Poiseuille flow.

Correspondence to: G. J. Hwang, Department of Power Mechanical Engineering, National Tsing Hua University, Hsinchu, 30043, Taiwan.

CCC 0271–2091/98/040443–15 $17.50

*Received December 1996*
*Revised April 1997*

Classical Orr–Sommerfeld theory deals with the stability of linear Tollmien–Schlichting (T–S) waves with a definite wave number or frequency at a given Reynolds number. Thoms[1] solved earlier theoretical work and obtained a critical Reynolds number $Re_c$ of about 3853·33, where $Re$ is based on the mean velocity and the channel half-height. Orszag[2] investigated the linear stability of the temporal Orr–Sommerfeld eigenmodes and predicted the critical Reynolds number to be 3848·15.

Grosch and Salwen[3] integrated the linearized equations though one period of oscillation. Herbert[4] carried out an energy analysis for small modulation amplitudes. He inspected the energy transfer process in the thin shear layer near the wall and emphasized the importance of the interaction of the unsteady portion of the mean flow with the disturbance. Hall[5] investigated the stability characteristics of oscillatory plane Poiseuille flow for high-frequency modulations and concluded that the high-frequency oscillations have a slightly destabilizing effect. Von Kerczek[6] accomplished a perturbation analysis of the linear equations about the critical Reynolds number and discovered that the modulation frequencies stabilize the flow. Singer *et al.*[7] studied the effect of flow oscillation on the stability of plane channel flow via numerical simulation. They found that the maximum growth rates occur when the instantaneous velocity profile has large regions of positive curvature.

Fasel[8] proposed an implicit finite difference scheme with a three-point difference for the time derivative and central differences for space derivatives to investigate the stability of a semi-infinite flat plate producing Tollmien–Schlichting waves. Moreover, Fasel and Bestek[9] investigated the non-linear effects of spatial disturbance amplification in plane Poiseuille flow by the same numerical method. Orszag and Kells[10] also proposed the direct numerical solution of the three-dimensional time-dependent Navier–Stokes equations for the evolution of finite amplitude disturbance by spectral methods.

On the other hand, Nishioka *et al.*[11] performed experiments in a laminar plane Poiseuille flow with delay-critical Reynolds number $Re = 5333{\cdot}33$, where $Re = U_m h/v$. They had to reduce the background turbulence level to less than 0·05%, because instabilities were obtained at lower Reynolds numbers at larger disturbance levels. Recent experiments on plane Poiseuille flow, such as those by Carlson *et al.*[12] and Alavyoon *et al.*,[13] have shown that the Reynolds number of the experimental transition is much lower than the theoretical prediction for instability in plane Poiseuille flow. This implies that the disturbances can grow below the critical Reynolds number of linear theory provided that their amplitudes lie above some threshold value. It seems necessary to undertake also a non-linear analysis for subcritical Reynolds numbers.

In the present paper a direct numerical scheme is applied to study the temporal amplification of a two-dimensional disturbance in plane Poiseuille flow. The transient non-linear Navier–Stokes equations are applied in a region of wavelength moving with the wave propagation speed. In this study a fully implicit finite difference scheme with five points in the flow direction and three points in the normal direction is developed. It is expected that the critical conditions marking the onset of T–S waves obtained by the present numerical scheme can be compared with existing solutions of linear stability theory. By fixing the wavelength and increasing the Reynolds number, the non-linear disturbance solution with finite amplitudes can be obtained to study the non-linear flow characteristics in the supercritical regime. The critical conditions for the amplitude of various disturbance levels are also studied.

## 2. THEORETICAL ANALYSIS

Consider a fully developed flow in a parallel plate channel with a gap $2h$. The dimensional velocities for the basic flow are

$$\hat{u}_b = \tfrac{3}{2} U_m (1 - \hat{y}^2/h^2), \qquad \hat{v}_b = 0, \tag{1}$$

 

where $U_m$ is the mean velocity of the basic flow and the superscript 'hat' denotes a dimensional variable. When the Reynolds number $Re = U_m h/v$ is higher than a certain value, two-dimensional T–S waves may be generated and propagated along the flow direction as shown in Figure 1. Viewing the wave motion from a fixed point on the ground (i.e. $\hat{x}$–$\hat{y}$ co-ordinates), the flow appears unsteady to a stationary observer. However, the flow is steady to an observer located on a frame moving with the wave propagation speed $c_r$. Consequently, the co-ordinate transformations between the $\hat{X}$–$\hat{Y}$ and $\hat{x}$–$\hat{y}$ frames are $\hat{X} = \hat{x} - c_r\hat{t}$ and $\hat{Y} = \hat{y}$.

### 2.1. Perturbation equations

The perturbation quantities are superimposed on the basic flow quantities as

$$\hat{u} = \hat{u}_b(\hat{y}) + \hat{u}'(\hat{x}, \hat{y}, \hat{t}), \qquad \hat{v} = \hat{v}'(\hat{x}, \hat{y}, \hat{t}), \qquad \hat{p} = \hat{p}_b(\hat{x}) + \hat{p}'(\hat{x}, \hat{y}, \hat{t}). \tag{2}$$

The above perturbation quantities are considered as functions of space variables $\hat{x}, \hat{y}$ and time $\hat{t}$. By substituting the resultant velocity and pressure into the conservation equations for mass and momentum and subtracting the equations for the basic flow quantities, we obtain the perturbation equations

$$\frac{\partial \hat{u}'}{\partial \hat{x}} + \frac{\partial \hat{v}'}{\partial \hat{y}} = 0, \tag{3}$$

$$\frac{\partial \hat{u}'}{\partial \hat{t}} + \hat{u}_b \frac{\partial \hat{u}'}{\partial \hat{x}} + \hat{v}' \frac{\partial \hat{u}_b}{\partial \hat{y}} + \hat{u}' \frac{\partial \hat{u}'}{\partial \hat{x}} + \hat{v}' \frac{\partial \hat{u}'}{\partial \hat{y}} = -\frac{1}{\rho}\frac{\partial \hat{p}'}{\partial \hat{x}} + v\left(\frac{\partial^2 \hat{u}'}{\partial \hat{x}^2} + \frac{\partial^2 \hat{u}'}{\partial \hat{y}^2}\right), \tag{4}$$

$$\frac{\partial \hat{v}'}{\partial \hat{t}} + \hat{u}_b \frac{\partial \hat{v}'}{\partial \hat{x}} + \hat{u}' \frac{\partial \hat{v}'}{\partial \hat{x}} + \hat{v}' \frac{\partial \hat{v}'}{\partial \hat{y}} = -\frac{1}{\rho}\frac{\partial \hat{p}'}{\partial \hat{y}} + v\left(\frac{\partial^2 \hat{v}'}{\partial \hat{x}^2} + \frac{\partial^2 \hat{v}'}{\partial \hat{y}^2}\right). \tag{5}$$

Then, introducing the dimensionless variables and parameters

$$\hat{x} = [h]x, \qquad \hat{y} = [h]y, \qquad \hat{u}' = [U_m]u, \qquad \hat{v}' = [U_m]v,$$
$$\hat{u}_b = [U_m]u_b, \qquad \hat{t} = [h/U_m]t, \qquad \hat{p}' = [\rho U_m^2]p, \qquad Re = U_m h/v,$$

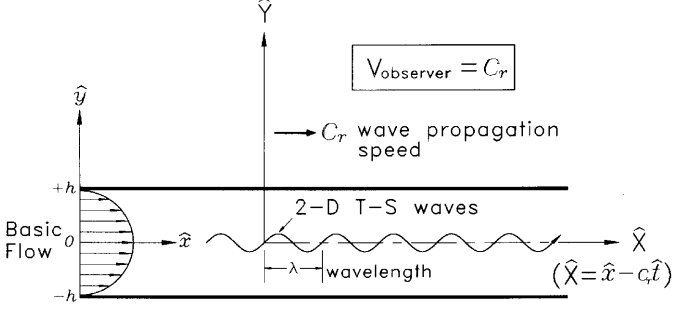


Figure 1. Schematic diagram of physical system

 

the dimensionless perturbation equations become

$$\frac{\partial u}{\partial x}+\frac{\partial v}{\partial y}=0, \tag{6}$$

$$\frac{\partial u}{\partial t}+u_{\mathrm{b}}\frac{\partial u}{\partial x}+v\frac{\partial u_{\mathrm{b}}}{\partial y}+u\frac{\partial u}{\partial x}+v\frac{\partial u}{\partial y}=-\frac{\partial p}{\partial x}+\frac{1}{Re}\left(\frac{\partial^2 u}{\partial x^2}+\frac{\partial^2 u}{\partial y^2}\right), \tag{7}$$

$$\frac{\partial v}{\partial t}+u_{\mathrm{b}}\frac{\partial v}{\partial x}+u\frac{\partial v}{\partial x}+v\frac{\partial v}{\partial y}=-\frac{\partial p}{\partial y}+\frac{1}{Re}\left(\frac{\partial^2 v}{\partial x^2}+\frac{\partial^2 v}{\partial y^2}\right), \tag{8}$$

where

$$u_{\mathrm{b}}=\tfrac{3}{2}(1-y^2). \tag{9}$$

Subsequently, we define the vorticity $\omega$ and streamfunction $\psi$ as

$$\omega=\frac{\partial u}{\partial y}-\frac{\partial v}{\partial x} \tag{10}$$

and

$$u=\frac{\partial \psi}{\partial y}, \qquad v=-\frac{\partial \psi}{\partial x}. \tag{11}$$

For the numerical solution the Navier–Stokes equations are transformed to the vorticity transport form by eliminating the pressure terms via a cross-differentiation process as follows:

$$\frac{\partial \omega}{\partial t}+u_{\mathrm{b}}\frac{\partial \omega}{\partial x}-\frac{\partial \psi}{\partial x}\frac{\mathrm{d}^2 u_{\mathrm{b}}}{\mathrm{d}y^2}+\frac{\partial \psi}{\partial y}\frac{\partial \omega}{\partial x}-\frac{\partial \psi}{\partial x}\frac{\partial \omega}{\partial y}=\frac{1}{Re}\left(\frac{\partial^2 \omega}{\partial x^2}+\frac{\partial^2 \omega}{\partial y^2}\right), \tag{12}$$

where

$$\omega=\frac{\partial^2 \psi}{\partial x^2}+\frac{\partial^2 \psi}{\partial y^2}, \qquad \frac{\mathrm{d}^2 u_{\mathrm{b}}}{\mathrm{d}y^2}=\frac{\mathrm{d}}{\mathrm{d}y}\left(\frac{\mathrm{d}u_{\mathrm{b}}}{\mathrm{d}y}\right)=\frac{\mathrm{d}}{\mathrm{d}y}(-3y)=-3.$$

Moreover, transforming the fixed co-ordinates $(x, y, t)$ to moving co-ordinates $(X, Y, t)$, i.e. letting $X=x-c_{\mathrm{r}}t$, one obtains the following equations in the $X$–$Y$ plane for the time-dependent non-linear effect:

$$\frac{\partial \omega}{\partial t}+(u_{\mathrm{b}}-c_{\mathrm{r}})\frac{\partial \omega}{\partial X}+3\frac{\partial \psi}{\partial X}+\frac{\partial \psi}{\partial Y}\frac{\partial \omega}{\partial X}-\frac{\partial \psi}{\partial X}\frac{\partial \omega}{\partial Y}=\frac{1}{Re}\left(\frac{\partial^2 \omega}{\partial X^2}+\frac{\partial^2 \omega}{\partial Y^2}\right), \tag{13}$$

$$\frac{\partial^2 \psi}{\partial X^2}+\frac{\partial^2 \psi}{\partial Y^2}=\omega. \tag{14}$$

The numerical computation is then based on (13) and (14) with appropriate initial and boundary conditions which are specified below in detail. It has been reported from the so-called Squire's theorem[14] that two-dimensional disturbances are always more unstable to plane Poiseuille flow than three-dimensional ones; thus the present two-dimensional model may be appropriate in this study.

### 2.2. *Initial and boundary conditions*

The appropriate initial and boundary conditions of the perturbation quantities are as follows.

*Initial conditions.* The results obtained from linear stability theory is used for the initial condition. The neutral stability solutions including $\phi_{\mathrm{r}}$, $\phi_{\mathrm{i}}$, $W_{\mathrm{r}}$ and $W_{\mathrm{i}}$ are depicted in Figure 2 for $Re=3853$, $\alpha=1{\cdot}02$ and $c_{\mathrm{r}}=0{\cdot}395642$, where the subscripts 'r' and 'i' denote respectively the real and imaginary parts of the solution from linear stability theory.[15]

 

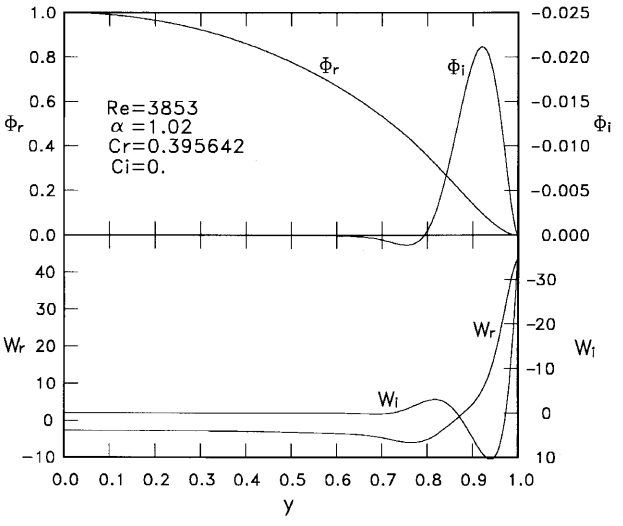


Figure 2. Eigenfunctions at $\alpha = 1{\cdot}02$, $Re = 3853$ and $c_r = 0{\cdot}395642$ used as initial condition for plane Poiseuille flow stability

The initial conditions of $\psi$ and $\omega$ in (13) and (14) can be evaluated as

$$\psi(X, Y, 0) = \frac{A_0}{N}[\phi_r(Y)\cos(\alpha X) - \phi_i(Y)\sin(\alpha X)], \tag{15}$$

$$\omega(X, Y, 0) = \frac{A_0}{N}[W_r(Y)\cos(\alpha X) - W_i(Y)\sin(\alpha X)], \tag{16}$$

where $\alpha = 2\pi/\lambda$ is the dimensionless wave number, $N$ is the 'normalization factor', defined as

$$N = \left(\frac{1}{2\lambda}\int_0^{\lambda}\int_{-1}^{1}[\phi_r(Y)\cos(\alpha X) - \phi_i(Y)\sin(\alpha X)]^2\,\mathrm{d}Y\,\mathrm{d}X\right)^{1/2}, \tag{17}$$

and $A_0$ is the initial magnitude of disturbance.

*Boundary conditions*

$$\frac{\partial^2\omega}{\partial X^2} = -\alpha^2\omega \quad \text{and} \quad \frac{\partial^2\psi}{\partial X^2} = -\alpha^2\psi \qquad \text{at } X = 0, X = \lambda \quad \text{and} \quad -1 \leqslant Y \leqslant 1, \tag{18a}$$

$$\omega = \frac{\partial^2\psi}{\partial Y^2} \quad \text{and} \quad \psi = 0 \qquad \text{at } Y = -1 \quad \text{and} \quad 0 \leqslant X \leqslant \lambda \tag{18b}$$

$$\omega = \frac{\partial^2\psi}{\partial Y^2} \quad \text{and} \quad \psi = 0 \qquad \text{at } Y = 1 \quad \text{and} \quad 0 \leqslant X \leqslant \lambda. \tag{18c}$$

For determining the growth or decay of the disturbance with time, the root mean square value of the instantaneous perturbation streamfunction is defined as

$$A_n = \left(\frac{1}{2\lambda}\int_0^{\lambda}\int_{-1}^{1}[\psi(X, Y, t)]^2\,\mathrm{d}Y\,\mathrm{d}X\right)^{1/2}. \tag{19}$$

 

For $n = 0$,

$$A_0 = \left( \frac{1}{2\lambda} \int_0^{\lambda} \int_{-1}^{1} [\psi(X, Y, 0)]^2 \, \mathrm{d}Y \, \mathrm{d}X \right)^{1/2}$$

is the initial magnitude of disturbance.

## 3. NUMERICAL METHOD AND SOLUTION

As mentioned above, there are two significant problems remaining to be solved. The first is to search for appropriate functions $\phi_r$, $\phi_i$, $W_r$ and $W_i$ as initial conditions. The second is to develop a numerical scheme to investigate the transient non-linear stability equations.

### *3.1. Linear stability equation for initial conditions*

We reduce the fourth-order Orr–Sommerfeld equation with non-constant coefficients to a set of second-order differential equations

$$(D^2 - \alpha^2)W_r = -\alpha \, Re[(u_b - c_r)W_i + 3\phi_i - c_i w_r], \tag{20}$$

$$(D^2 - \alpha^2)W_i = \alpha \, Re[(u_b - c_r)W_r + 3\phi_r - c_i w_i], \tag{21}$$

$$(D^2 - \alpha^2)\phi_r = W_r, \tag{22}$$

$$(D^2 - \alpha^2)\phi_i = W_i, \tag{23}$$

where $D$ denotes $\mathrm{d}/\mathrm{d}Y$, $\phi_r$ and $\phi_i$ are the real and imaginary parts of amplitude functions of the perturbation streamfunction respectively and $W_r$ and $W_i$ are the real and imaginary parts of amplitude functions of the perturbation vorticity respectively. These are functions of $Y$ only.

For simplicity, only half of the gap is taken for computation. The associated boundary conditions are

$$\phi_r(1) = \phi_i(1) = \phi_r'(1) = \phi_i'(1) = 0, \qquad W_r(1) = \phi_r''(1), \qquad W_i(1) = \phi_i''(1), \tag{24}$$

$$\phi_r'(0) = \phi_i'(0) = 0, \qquad W_r'(0) = W_i'(0) = 0. \tag{25}$$

We let $\phi_r(0) = 1$ and $\phi_i(0) = 0$, whereby the eigenfunction is normalized. The boundary conditions for $\phi$ are obtained by considering the no-slip and no-suction/blowing conditions. The conditions for $W$ in (24) are obtained by the definition of vorticity. The conditions for $W'$ in (25) are obtained by the symmetry condition.

Equations (20–(23) together with boundary conditions (24) and (25) comprise a system of algebraic equations which can be written in the form

$$[\mathbf{A}][\mathbf{x}] = [\mathbf{B}]. \tag{26}$$

The matrix $[\mathbf{A}]$ is function of $\alpha, c_r, c_i$ and $Re$; the vector $[\mathbf{B}]$ is a non-zero $[4 \times (n-1))$-dimensional array. In solving the eigenvalue problem, one assigns two of these values, say $Re$ and $c_i$, and guesses the remaining two, say $\alpha$ and $c_r$, and then solves equation (26) by the Gaussian

 

elimination method. Next, the eigenvalues $\alpha^{k+1} = \alpha^k + \Delta\alpha$ and $c_r^{k+1} = c_r^k + \Delta c_r$ are adjusted by the two-dimensional secant method[16] to determine $\Delta\alpha$ and $\Delta c_r$, which is described by the equations

$$\phi_r(0) + \frac{\partial \phi_r(0)}{\partial \alpha}\Delta\alpha + \frac{\partial \phi_r(0)}{\partial c_r}\Delta c_r = 1, \tag{27}$$

$$\phi_i(0) + \frac{\partial \phi_i(0)}{\partial \alpha}\Delta\alpha + \frac{\partial \phi_i(0)}{\partial c_i}\Delta c_i = 0, \tag{28}$$

until the conditions $\phi_r(0) = 1$ and $\phi_i(0) = 0$ are satisfied within a prescribed tolerance. It is noted that on the curve of $\alpha$ versus $Re$ for neutral stability, $c_i$ can be assigned a value of zero.

Table I shows the results of the present method with different grid numbers ($n = 60$, 100, 200) in comparison with the classical result of Thomas[1] for $Re = 6666{\cdot}67$, $\alpha = 1$ flow. It is obvious that the result for the case $n = 200$ is quite close to that of Thomas. Therefore a grid number of 400 in the $Y$-direction is used for the full gap in the subsequent computation.

### 3.2. Discretization of transient non-linear N–S equation

The transient non-linear perturbation equation (13) is essentially a mixed parabolic–elliptic eigenvalue-type differential equation that includes a time-dependent term, convective terms, and diffusive terms. It is noted that the functions $\psi$ and $\omega$ must be self-excited, because there is no 'source term' in (13). In the present study, a Crank–Nicolson scheme with truncation error of $O[(\Delta t)^2]$ is used for time marching. Time steps $\Delta t = 0{\cdot}01$, $0{\cdot}05$ and $0{\cdot}1$ were tested. Finally, $\Delta t = 0{\cdot}05$ (corresponding to a real time step of about $0{\cdot}002$ s for $Re = 10{,}000$ in the present study) was selected by consideration of both the accuracy of the transient solution and the computation time required to reach the steady state solution. Note that the selection of $\Delta t$ is not sensitive to the steady state solution. The time derivative $\partial\omega/\partial t$ in (13) can be written as

$$\frac{\omega_{i,j}^n - \omega_{i,j}^{n-1}}{\Delta t} = \frac{1}{2}\left[\left(\frac{\partial \omega}{\partial t}\right)_{i,j}^{n} + \left(\frac{\partial \omega}{\partial t}\right)_{i,j}^{n-1}\right]. \tag{29}$$

Table I. Numerical experiment for solution of Orr–Sommerfeld equation in plane Poiseuille flow ($Re = 6666{\cdot}67$, $\alpha = 1{\cdot}0$)

| | | No of nodes in $Y$-direction | | | |
|---|---|---|---|---|---|
| | $Y$ | $n = 60$ | $n = 100$ | $n = 200$ | Thomas[1] |
| $\phi_r$ | 0·1 | 0·991894 | 0·991877 | 0·991869 | 0·991868 |
| | 0·3 | 0·925735 | 0·925581 | 0·925517 | 0·925497 |
| | 0·5 | 0·785872 | 0·785432 | 0·785248 | 0·785190 |
| | 0·7 | 0·553009 | 0·552087 | 0·551702 | 0·551578 |
| | 0·9 | 0·168899 | 0·167395 | 0·166768 | 0·166567 |
| $\phi_i$ | 0·2 | −0·000058 | −0·000063 | −0·000064 | −0·000064 |
| | 0·3 | −0·000527 | −0·000570 | −0·000583 | −0·000584 |
| | 0·5 | −0·001497 | −0·001621 | −0·001658 | −0·001662 |
| | 0·7 | −0·003002 | −0·003259 | −0·003335 | −0·003346 |
| | 0·9 | −0·018771 | −0·018979 | −0·018998 | −0·018982 |
| $c_r$ | | 0·354047 | 0·355490 | 0·356251 | 0·356289 |
| $c_i$ | | 0·005061 | 0·005461 | 0·005577 | 0·005611 |

It is seen in the convective terms of (13) that the coefficients $u_b - c_r + \partial\psi/\partial Y$ of $\partial\omega/\partial X$ are positive near the centre and negative near the channel wall. To enhance the numerical stability and yield accurate results, a third-order five-point upwind scheme,[17] shown in Figure 3, is employed to discretize the convective term:

$$\left(U^* \frac{\partial\omega}{\partial X}\right)_{i,j} = U^*_{i,j} \frac{-\omega_{i+2,j} + 8\omega_{i+1,j} - 8\omega_{i-1,j} + \omega_{i-2,j}}{12\Delta X} + |U^*_{i,j}| \frac{3\omega_{i+2,j} - 12\omega_{i+1,j} + 18\omega_{i,j} - 12\omega_{i-1,j} + 3\omega_{i-2,j}}{12\Delta X}, \tag{30}$$

where $U^*_{i,j} = u_b - c_r + \partial\psi/\partial Y$. Regarding the $X$-direction second-order derivative $\partial^2\omega/\partial X^2$, the five-point central difference scheme is applied. For the $Y$-direction derivatives the power-law scheme of Patankar is employed. The calculation was carried out iteratively from upstream to downstream as shown in Figure 3.

Before the numerical scheme was developed, the three-point power-law scheme of Patanker was also tested. Owing to the large truncation error in the three-point scheme, which may be greater than the magnitude of the major stabilizing viscous term $(\partial^2\omega/\partial X^2 + \partial^2\omega/\partial Y^2)/Re$ in (13), the functions $\psi$ and $\omega$ cannot be self-excited even with large initial magnitudes of $\psi$ and $\omega$. The selection of a proper discretization scheme is the key to the success of this study.

Since the wave propagation speed $c_r$ changes with $Re$ and $\alpha$, one must correct $c_r$ to avoid the shift of T–S waves during the computation. The correction $\Delta c_r$ is set as

$$\Delta c_r = \frac{X_{new} - X_{old}}{t_{new} - t_{old}}. \tag{31}$$

By using cubic spline interpolation, one can find the location $(X_{old}, 0)$ of the maximum perturbation streamfunction $\psi_{max}$ at $t = t_{old}$ and the new location $(X_{new}, 0)$ at $t = t_{new}$. The time interval $t_{new} - t_{old}$ is selected as 10 times $\Delta t$ in the present study.

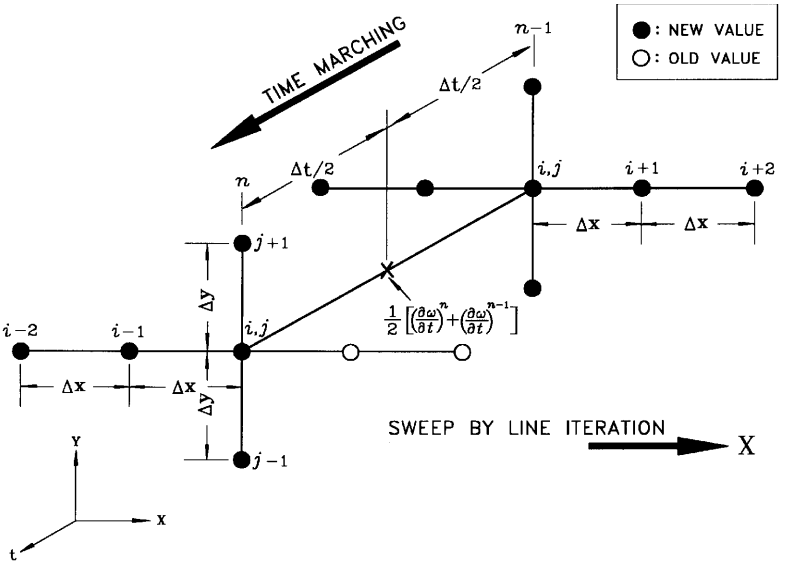


Figure 3. Finite difference scheme

 

Table II. Grid test for $Re = 5000$ and $\alpha = 1{\cdot}02$ at $t = 50$ and 100

| | Grid size | $c_r$ | $A_n$ | $\overline{f\,Re}$ |
|---|---|---|---|---|
| $t = 50$ | $80 \times 400$ | 0·392186 | 0·012941 | 24·426 |
| | $60 \times 400$ | 0·391895 | 0·012904 | 24·424 |
| | $40 \times 400$ | 0·391159 | 0·012803 | 24·418 |
| | $20 \times 400$ | 0·388849 | 0·011453 | 24·354 |
| $t = 100$ | $80 \times 400$ | 0·399372 | 0·017413 | 24·729 |
| | $60 \times 400$ | 0·398964 | 0·017298 | 24·720 |
| | $40 \times 400$ | 0·398474 | 0·016981 | 24·698 |
| | $20 \times 400$ | 0·389619 | 0·013204 | 24·448 |

The local friction factor $f\,Re$ and the average friction factor $\overline{f\,Re}$ in plane Poiseuille flow are defined as

$$f\,Re = 8\left(\frac{\mathrm{d}u_b}{\mathrm{d}Y} + \frac{\partial u}{\partial Y}\right)_{\text{wall}} = \begin{cases} 24 + 8\dfrac{\partial^2 \psi}{\partial Y^2}\bigg|_{y=-1} = 24 + 8\omega|_{Y=-1} & \text{(lower plate)}, \\ 24 - 8\dfrac{\partial^2 \psi}{\partial Y^2}\bigg|_{Y=1} = 24 - 8\omega|_{Y=1} & \text{(upper plate)}, \end{cases} \tag{32}$$

$$\overline{f\,Re} = \frac{1}{\lambda}\int_0^{\lambda} f\,Re\,\mathrm{d}X, \tag{33}$$

where $Re = U_m h/v$.

As shown in Table II, a spatial grid test for $Re = 5000$ and $\alpha = 1{\cdot}02$ was carried out. It is seen that the average friction factor $\overline{f\,Re}$ for the $60 \times 400$ grid deviates from that for the $80 \times 400$ grid by less than 0·01% at $t = 50$ and 0·04% at $t = 100$. Therefore grid dimensions of $60 \times 400$ are used throughout the computation.

## 4. RESULTS AND DISCUSSION

Taking an initial magnitude of disturbance $A_0 = 0{\cdot}001$, the full lines in Figure 4 show the effect of $Re$ on the growth and decay of the disturbance with time. When $Re = Re_c = 3853$, the magnitude of disturbance is insensitive to the variation in time. When $Re = 3900 > Re_c$, the magnitude grows with time. In contrast, when $Re = 3810 < Re_c$, the magnitude decays with time. Eliminating the non-linear terms in (13), the broken lines in Figure 4 show the growth and decay of the disturbance without the non-linear effect when $Re \approx Re_c$. It is seen that the non-linear terms have little effect on the growth and decay of the disturbance when its magnitude is small.

Next, taking initial magnitudes of disturbance $A_0 = 0{\cdot}0001$, 0·006 and 0·01, the results are shown in Figure 5. When $A_0 = 0{\cdot}0001$, the marginal stability curve of the non-linear equation is nearly coincident with that of the linear ordinary differential equation. The curves of marginal stability for $A_0 = 0{\cdot}006$ and 0·01 are shifted from that for $A_0 = 0{\cdot}0001$. It is seen that the curves of marginal stability for the various initial magnitudes of disturbance intersect at point B (about $Re = 4266$, $\alpha = 0{\cdot}936$). The upper branch of the neutral curves above point B for finite amplitudes lies in the zone which is stable to infinitesimal disturbances, while the lower portion of the neutral curves below point B for finite amplitudes lies inside the unstable zone. The present results are just like those drawn schematically by Pekeris and Shkoller.[18]

 

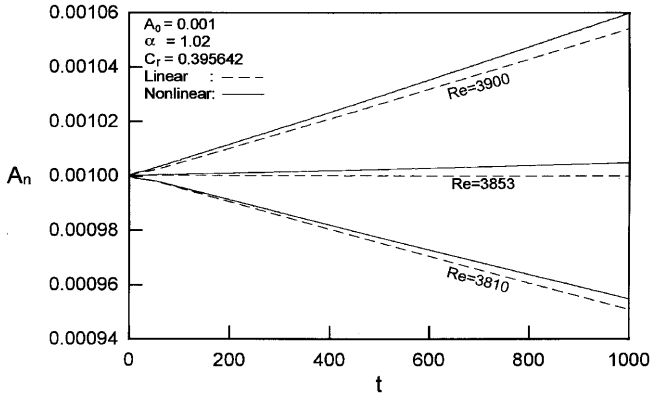


Figure 4. Amplification and decay of streamfunction

Figure 6 shows the critical Reynolds number, together with the corresponding wave number and dimensionless frequency, as a function of the initial magnitude of disturbance. The results are in agreement with those of Pekeris and Shkoller.[18] In fact, the present data may explain why the critical Reynolds number obtained in the experiments is less than the prediction by linear theory. The nonlinear effect caused by the finite initial disturbance destablizes the flow.

In the present study we assume that the wave number $\alpha$ is fixed once the initial disturbance has developed. The computation in the post-critical regime keeping $\alpha$ fixed has also been done for vortex rolls in a thermal instability problem. It may be interesting to see the development of the friction factors with the initial input magnitude. Figure 7 shows the time trends of $A_n$ and $\overline{f\,Re}/(\overline{f\,Re})_0$ for $A_0 = 0{\cdot}001$, $0{\cdot}01$ and $0{\cdot}05$. It is seen that a large initial input produces large initial growth rates for both $A_n$ and $\overline{f\,Re}/(\overline{f\,Re})_0$. An overshoot of $\overline{f\,Re}/(\overline{f\,Re})_0$ is observed for $A_0 = 0{\cdot}05$ at $t \approx 80$, though no sign of overshoot is found for $A_0$. At $t = 2000$ all curves of $A_n$ and $f\,Re/(\overline{f\,Re})_0$ meet

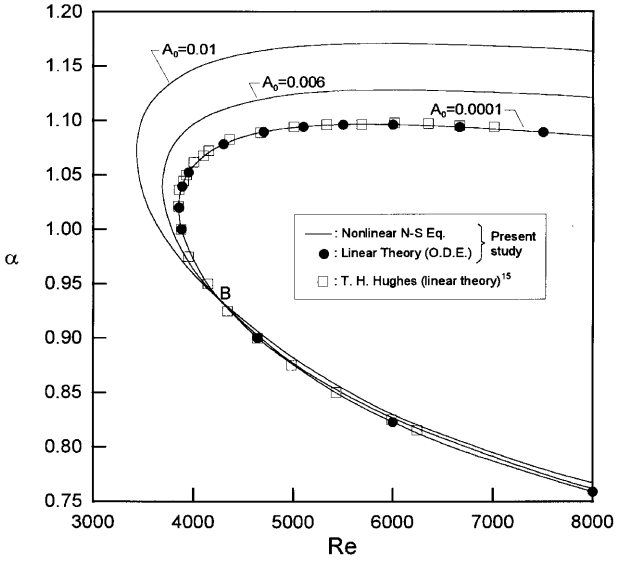


Figure 5. Comparison of curves of marginal stability for plane Poiseuille flow

 

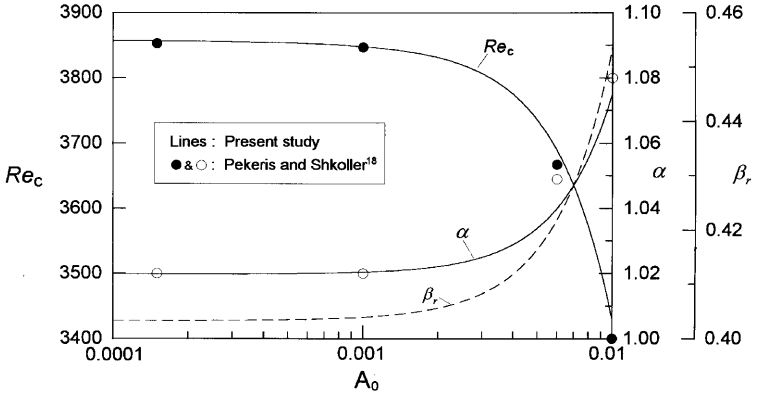


Figure 6. Critical conditions: $Re_c$, $\alpha$ and $\beta_r$ $(= \alpha c_r)$ as functions of $A_0$

asymptotically. A large initial input leads to the final asymptotic value being approached earlier than with a small initial input. This suggests the use of larger $A_0$ for the computation of $\overline{f\,Re}/(\overline{f\,Re})_0$ in the post-critical regime. In the present study, $A_0 = 0{\cdot}01$ was used for the evaluation of $\overline{f\,Re}/(\overline{f\,Re})_0$ in Figure 10.

Figure 8 depicts the streamfunction of disturbance, streamlines, vorticity and velocity vector for $Re = 10{,}000$, $\alpha = 1{\cdot}02$ and $c_r = 0{\cdot}566068$. It is seen that the streamfunction of disturbance in Figure 8(a) is no longer sinusoidal along the flow direction. The streamlines in Figure 8(b) combine the main flow and the perturbation velocity. It is seen in the plots of streamlines, vorticity and velocity vector in Figures 8(b)–8(d) that a wavy motion occurs in the flow direction. It is observed that weak reversed flows of pitch $\lambda$ appear alternately at the upper and lower walls in the plot of streamlines. In the plot of vorticity, oval-shaped constant-vorticity lines are also seen near the region of reversed flow.

To the authors' knowledge, the distribution of friction factor indicating the flow characteristics along the lower and upper plates with non-linear T–S waves in plane Poiseuille flow has not yet been reported. If one closely examines the structure of vorticity contours within a wavelength, as shown in Figure 9, the flow reversal causes a negative value of $f\,Re$ on the upper plate for $X = 0$–$1{\cdot}8$ and $5{\cdot}8$–$6{\cdot}2$ and on the lower plate for $X = 2{\cdot}74$–$4{\cdot}8$. The maximum value of $f\,Re$ on the upper plate occurs at $X = 4{\cdot}8$, near the front of the upper flow reversal, while $f\,Re$ approximately equals zero on the lower

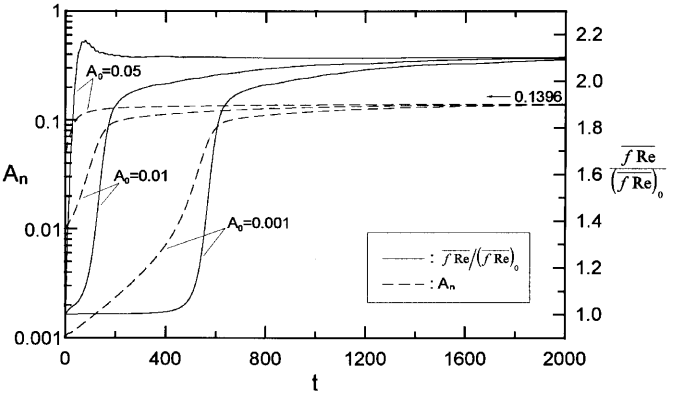


Figure 7. Time trends of $A_n$ and $\overline{f\,Re}/(\overline{f\,Re})_0$ for $Re = 10{,}000$, $\alpha = 1{\cdot}02$ and various $A_0$

 

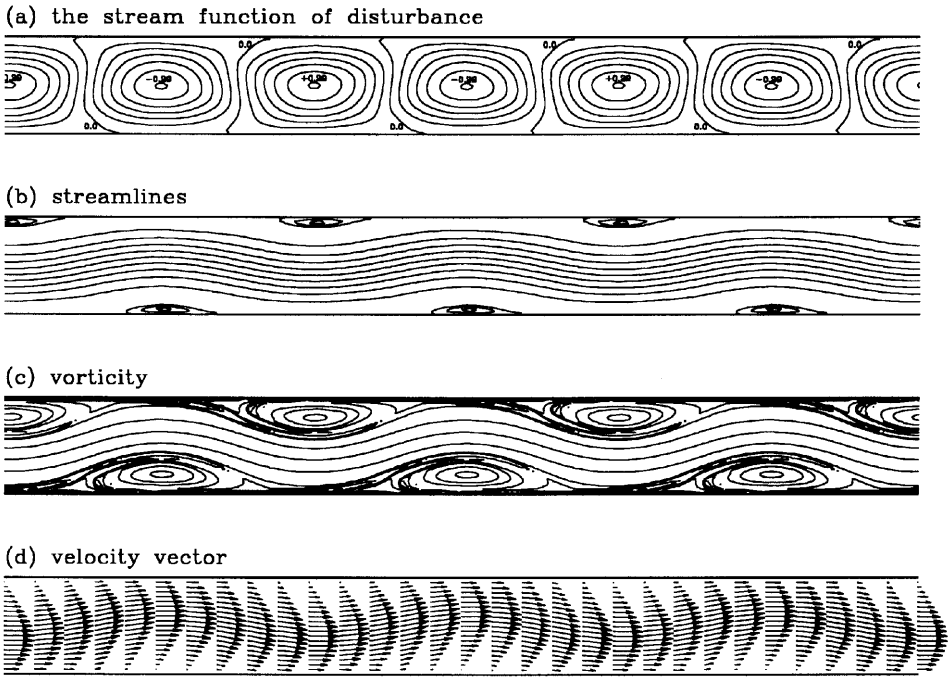


Figure 8. (a) Streamfunction of disturbance, (b) streamlines, (c) vorticity and (d) velocity vector in flow field for $Re = 10{,}000$, $\alpha = 1{\cdot}02$ and $c_r = 0.566068$

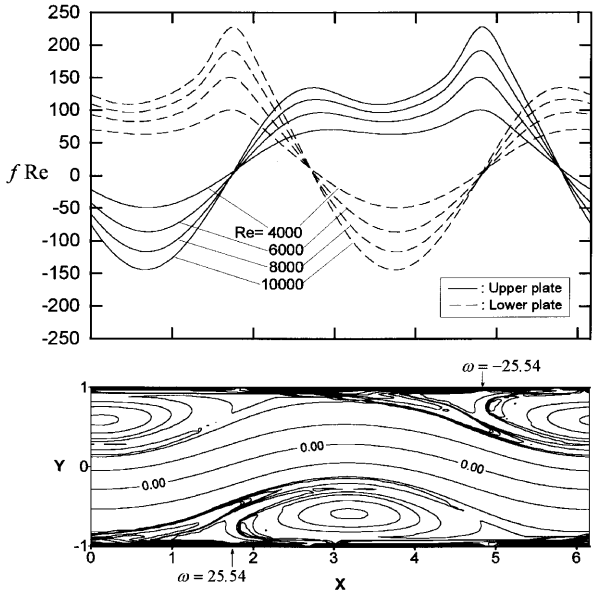


Figure 9. Local friction factor for $\alpha = 1{\cdot}02$ within a wavelength, contrasted with vorticity contours for $Re = 10{,}000$

 

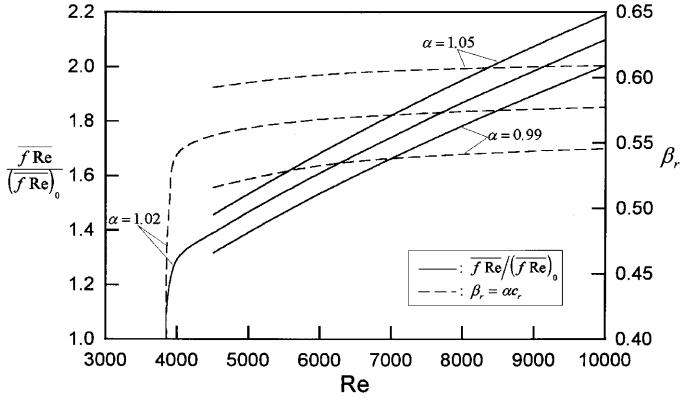


Figure 10. Amplification of average friction factor and dimensionless frequency for $Re > Re_c$ and various wave numbers with $(\overline{f\ Re})_0 = 24$ and $A_0 = 0{\cdot}0001$

plate. At this position of maximum $f\,Re$ the velocity distribution also shows a large velocity gradient near the wall, as observed in Figure 8(d). It is seen that the curve for the lower plate is identical to but shifted by $\lambda/2$ from that for the upper plate shown in Figure 9.

Although positive and negative values are seen in the local distribution of friction factor in Figure 9, the average friction factor may increase with increasing $Re$. Figure 10 shows the computed $\overline{f\ Re}/(\overline{f\ Re})_0$ and dimensionless frequency $\beta_r$ for $A_0 = 0{\cdot}0001, Re > Re_c$ (i.e. 3853) and wave numbers $\alpha = 0{\cdot}99$, $1{\cdot}02$ and $1{\cdot}05$. The friction factor ratio increases rapidly and the dimensionless frequency increases slowly with increasing $Re$. The increases in friction factor ratio and dimensionless frequency are almost linear for $Re = 4500$–$10{,}000$. It is seen that the friction factor ratios and dimensionless frequencies for $\alpha = 0{\cdot}99$ and $1{\cdot}05$ are within $\pm 10\%$ of those for $\alpha = 1{\cdot}02$. This figure displays the characteristics of plane Poiseuille flow in laminar–turbulent transition.

## 5. CONCLUDING REMARKS

A direct numerical scheme is successfully developed to study the temporal amplification of a 2D disturbance in plane Poiseuille flow. The utilization of a five-point finite difference formula in the $X$-direction, which effectively eliminates the stabilizing truncation error in a three-point scheme, is the key to the success of this study.

By varying the initial amplitude of disturbance from $A_0 = 0{\cdot}0001$ to $0{\cdot}01$, the results of the present simulation show that the critical $Re_c$ decreases and the wave number $\alpha$ and the dimensionless frequency $\beta_r = \alpha c_r$ increase with increasing $A_0$. The predicted results agree with those of Pekeris and Shkoller.[18]

In the post-critical regime a wavy motion along the flow direction and flow reversal at the upper and lower plates are observed. Weak reversed flows of pitch $\lambda$ appear alternatively at the upper and lower walls. The reversed flow causes a negative value of friction factor.

Although positive and negative values are seen in the local distribution of friction factor, the average friction factor increases with increasing Reynolds number. In the computation of friction factor in the post-critical regime the value of $\alpha$ is kept unchanged. It may also be interesting to see the effect of $\alpha$ on the average friction factor. It is found that the friction factors for $\alpha = 0{\cdot}99$ and $1{\cdot}05$ are within $\pm 10\%$ of that for $\alpha = 1{\cdot}02$.

 

## APPENDIX: NOMENCLATURE

| | |
|---|---|
| $A_n$ | root mean square value of perturbation streamfunction |
| $A_0$ | initial magnitude of disturbance |
| $c_i$ | amplification factor |
| $c_r$ | dimensionless wave propagation speed, $\hat{c}_r/U_m$ |
| $f\,Re$ | local friction factor |
| $\overline{f\,Re}$ | average friction factor |
| $h$ | half of distance between two parallel plates (m) |
| $n$ | $Y$-direction grid index |
| $N$ | normalization factor defined in (17) |
| $p$ | dimensionless perturbation pressure |
| $Re$ | Reynolds number, $U_m h/v$ |
| $t$ | dimensionless time |
| $u, v$ | dimensionless streamwise and normal perturbation velocities |
| $u_b$ | dimensionless streamwise basic velocity |
| $U_m$ | streamwise mean velocity ($m\,s^{-1}$) |
| $W$ | amplitude function of perturbation vorticity |
| $x, y$ | dimensionless streamwise and normal stationary co-ordinates |
| $X, Y$ | dimensionless streamwise and normal co-ordinates moving with wave velocity $c_r$ in streamwise direction |

*Greek letters*

| | |
|---|---|
| $\alpha$ | wave number, $2\pi/\lambda$ |
| $\beta_r$ | dimensionless frequency, $\alpha c_r$ |
| $\Delta$ | difference |
| $\lambda$ | dimensionless wavelength, $2\pi/\alpha$ |
| $v$ | kinematic viscosity of fluid ($m^2\,s^{-1}$) |
| $\phi$ | amplitude function of perturbation streamfunction |
| $\psi$ | dimensionless perturbation streamfunction |
| $\omega$ | dimensionless perturbation vorticity |

*Superscripts*

| | |
|---|---|
| $k$ | iteration index |
| $n$ | number of time step |
| $()'$ | perturbation quantity |
| $(\hat{})$ | dimensional quantity |

*Subscripts*

| | |
|---|---|
| b | basic flow quantity |
| c | critical condition |
| i | imaginary part |
| m | mean flow |
| $n$ | time step index |
| r | real part |
| 0 | initial condition |

 

## REFERENCES


1. L. H. Thomas, 'The stability of plane Poiseuille flow', *Phys. Rev.*, 780–783 (1953).
2. S. A. Orszag, 'Accurate solution of the Orr–Sommerfeld stability equation', *J. Fluid Mech.*, **50**, 689–703 (1971).
3. C. E. Grosch and H. Salwen, 'The stability of steady and time-dependent plane Poiseuille flow', *J. Fluid Mech.*, **34**, 177–205 (1968).
4. D. M. Herbert, 'The energy balance in modulated plane Poiseuille flow', *J. Fluid Mech.*, **56**, 73–80 (1972).
5. P. Hall, 'The stability of Poiseuille flow modulated at high frequency', *Proc. R. Soc. Lond. A*, **344**, 453–464 (1975).
6. C. H. Von Kerczek, 'The instability of oscillatory plane Poiseuille flow', *J. Fluid Mech.*, **116**, 91–114 (1982).
7. B. A. Singer, J. H. Ferziger and H. L. Reed, 'Numerical simulations of transition in oscillatory plane channel flow', *J. Fluid Mech.*, **208**, 45–66 (1989).
8. H. Fasel, 'Investigation of the stability of boundary layers by a finite-difference model of the Navier–Stokes equations', *J. Fluid Mech.*, **78**, 355–383 (1976).
9. H. Fasel and H. Bestek, 'Investigation of nonlinear, spatial disturbance amplification in plane Poiseuille flow', *Proc. IUTAM Symp. on Laminar–Turbulent Transition*, Springer, New York, 1980, pp. 173–185.
10. S. A. Orszag and L. C. Kells, 'Transition to turbulence in plane Poiseuille and plane Couette flow', *J. Fluid Mech.*, **96**, 159–205 (1980).
11. M. Nishioka, S. Iida and Y. Ichikawa, 'An experimental investigation of the stability of plane Poiseuille flow', *J. Fluid Mech.*, **72**, 731–751 (1975).
12. D. R. Carlson, S. E. Widnall and M. F. Peters, 'A flow-visualization study of transition in plane Poiseuille flow', *J. Fluid Mech.*, **121**, 487–505 (1982).
13. F. Alavyoon, D. S. Henningson and P. H. Alfredsson, 'Turbulent spots in plane Poiseuille flow—flow visualization', *Phys. Fluids*, **29**, 1328–1331 (1986).
14. H. B. Squire, 'On the stability of three-dimensional distribution of viscous fluid between parallel walls', *Proc. Roy. Soc. Lond. A*, **142**, 621–628 (1933).
15. P. G. Drazin and W. H. Reid, *Hydrodynamic Stability*, Cambridge University Press, Cambridge, 1981, Chap. 4.
16. S. L. Lee, T. S. Chen and B. F. Armaly, 'New finite-difference solution methods for wave instability problems', *Numer. Heat Transfer*, **10**, 1–18 (1986).
17. T. Kawamura, H. Takami and K. Kawahara, 'New higher-order upwind scheme for incompressible Navier–Stokes equations', *Proc. 9th Int. Conf. on Numerical Methods in Fluid Dynamics*, Springer, New York, 1985, pp. 291–295.
18. C. L. Pekeris and B. Shkoller, 'The neutral curves for periodic perturbations of finite amplitude of plane Poiseuille flow', *J. Fluid Mech.*, **39**, 629–639 (1969).


 